Applied Physics Express

LETTER • OPEN ACCESS

Strain-induced reversible modulation of the magnetic anisotropy in perpendicularly magnetized metals deposited on a flexible substrate

To cite this article: Shinya Ota *et al* 2016 *Appl. Phys. Express* **9** 043004

OPEN ACCESS

Applied Physics Express **9**, 043004 (2016)

http://doi.org/**10.7567/APEX.9.043004**

Strain-induced reversible modulation of the magnetic anisotropy in perpendicularly magnetized metals deposited on a flexible substrate

Shinya Ota[1], Yuki Hibino[1], Do Bang[2], Hiroyuki Awano[2], Takahiro Kozeki[3], Hirokazu Akamine[3], Tatsuya Fujii[3], Takahiro Namazu[3], Taishi Takenobu[4,5,6], Tomohiro Koyama[1], and Daichi Chiba[1]

[1]*Department of Applied Physics, Faculty of Engineering, The University of Tokyo, Bunkyo, Tokyo 113-8656, Japan*
[2]*Toyota Technological Institute, Nagoya 468-8511, Japan*
[3]*Department of Mechanical and Systems Engineering, Division of Mechanical Systems, University of Hyogo, Himeji, Hyogo 671-2201, Japan*
[4]*Department of Applied Physics, Waseda University, Shinjuku, Tokyo 169-8555, Japan*
[5]*Department of Advanced Science and Engineering, Waseda University, Shinjuku, Tokyo 169-8555, Japan*
[6]*Kagami Memorial Laboratory for Material Science and Technology, Waseda University, Shinjuku, Tokyo 169-0051, Japan*

Received February 5, 2016; accepted February 22, 2016; published online March 14, 2016

In this study, the strain-induced change in the magnetic anisotropy of perpendicularly magnetized thin metals (TbFeCo and Pt/Co/Pt) deposited on a polyethylene naphthalate flexible substrate was investigated. The in-plane uniaxial tensile strain was reversibly applied up to 2%. The magnetic anisotropy was reversibly changed in both samples with applied stress. In the TbFeCo film, a marked change in magnetic anisotropy energy of 1.2×10^5 J/m^3 was observed. In the Pt/Co/Pt film, where the thickness of Co was 2–4 monolayers, the stress-induced changes in interface and volume contributions to magnetic anisotropy were individually determined. © 2016 The Japan Society of Applied Physics

The effects of stress on magnetic properties have been studied for a long time. In some magnetic films, the internal stress caused by lattice mismatch or film deposition is known to have important effects on the magnetic anisotropy (MA).[1,2] In recent years, multiple studies have dealt with the voltage control of magnetic properties in ferroelectric/ferromagnetic hybrid structures.[3–7] In such structures, the electric field on a ferroelectric material or piezo transducer generates a strain that affects magnetic properties via the inverse magnetostriction effect. However, the maximum strain applied to such stacks is limited by the performance of the ferroelectric material. This limitation on the strain reduces the possibility of a large modulation in magnetic properties. The use of an organic flexible substrate can eliminate this limitation. Some magnetic films,[8,9] including giant magnetoresistance devices,[10–12] tunneling magnetoresistance devices,[13,14] and spin Seebeck devices,[15] have been successfully formed on flexible substrates. One requirement for flexible devices is that their properties should not be changed after or while being strained. From another point of view, however, it would be interesting if their properties can be greatly modulated with a strain. In most bulk metals, plastic deformation occurs with a small strain on the order of 0.1%. When metals are in the form of a thin film, however, their yield strength increases,[16,17] and the flexible substrate/magnetic film structure becomes highly resilient.[17,18] For the in-plane magnetized films on flexible substrates, the conversion of the direction of the magnetic easy axis has been reported.[11] In this paper, we report on the strain-induced reversible modulation of the MA of perpendicularly magnetized TbFeCo (TFC) and Pt/Co/Pt films deposited on a poly(ethylene naphthalate) (PEN) substrate [Figs. 1(a) and 1(b)].

Two kinds of structures were deposited on 50-μm-thick PEN substrates by rf sputtering. The TFC sample consisted of Pt (4 nm)/TbFeCo (6 nm)/Pt (4 nm) layers. Sputtered TbFeCo is known to have an amorphous structure.[19] The TFC target was composed of 22.4 at. % Tb, 69.2 at. % Fe, and 8.3 at. % Co. The Pt/Co/Pt sample consisted of Ta (3 nm)/Pt (2 nm)/Co (t_{Co})/Pt (2 nm) layers from the substrate side, where the thickness of the Co layer was $t_{Co} = 0.4$–0.9 nm, which is much smaller than that of the TFC layer. Thus, the MA attributed to the Pt/Co interface was expected to be important for the perpendicular magnetic anisotropy (PMA) in this system. The X-ray diffraction peak by the (111) plane of an fcc Pt layer was clearly confirmed, when a Pt layer was deposited on a Si substrate with a Ta underlayer. The thicknesses of the layers were determined from the deposition rate of each material. The samples were cut into 3.5-mm-wide rectangular pieces, and the deposited layers were defined into 300-μm-wide Hall bar shapes [see the inset of Fig. 1(a)] by photolithography and Ar ion milling.

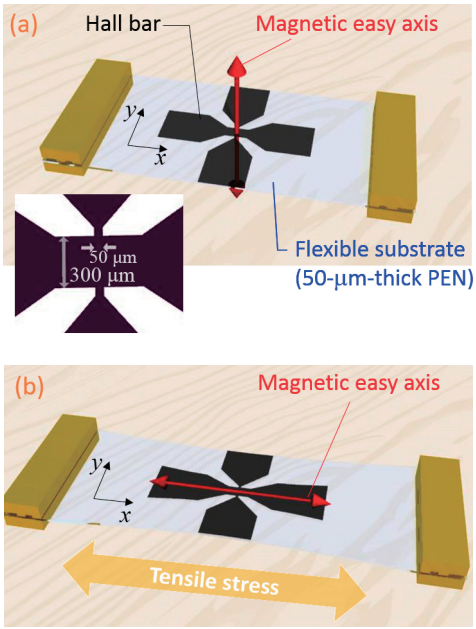

Fig. 1. Schematics of the Hall bar device formed on the flexible substrate. The red arrows indicate the magnetic easy axis switching from (a) the perpendicular direction before stress application to (b) the in-plane direction during stretching. The inset describes the scales of the Hall bar.

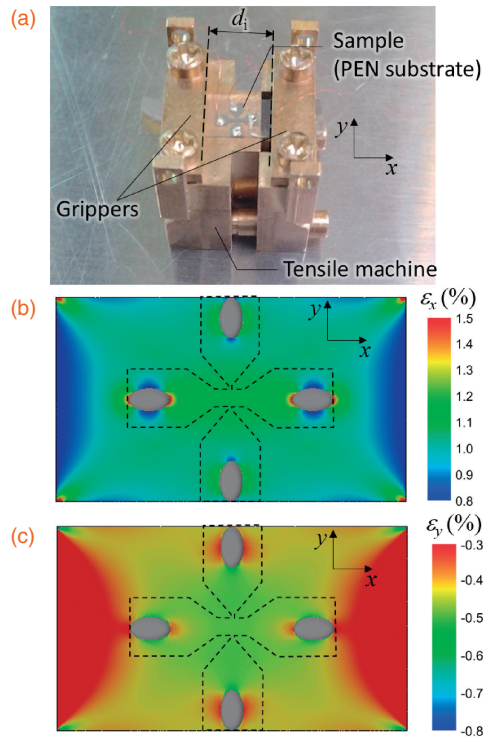

Fig. 2. (a) Sample piece with a Hall bar attached to the tensile machine. Distribution of the strains (b) parallel (ε_x) and (c) orthogonal (ε_y) to the applied stress calculated by FEM under a nominal strain of 1%. The strain in the epoxy is shown in gray because it is smaller than the color scale range.

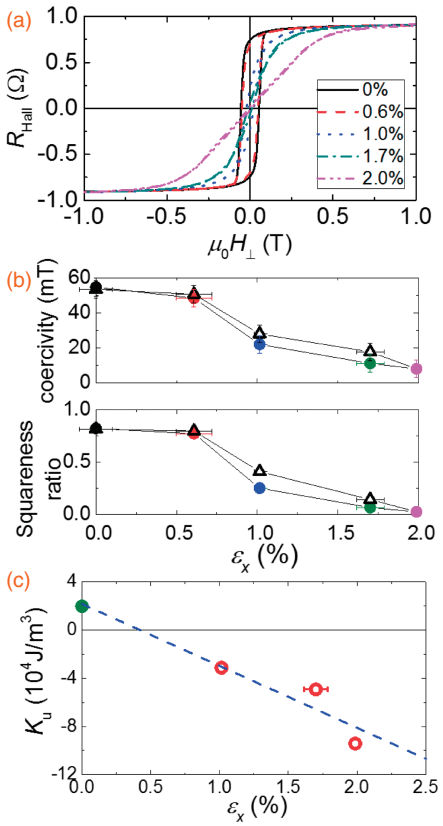

Fig. 3. (a) R_{Hall}–$H_\perp$ curve of the TFC sample under various strains. (b) Dependences of H_c and squareness ratio on ε_x. The filled circles and open triangles indicate the results measured while increasing and decreasing ε_x, respectively. The color of the filled circles corresponds to that of lines in (a). (c) K_u dependence on ε_x. The red open circles and a green filled circle were obtained from the R_{Hall}–$H_\perp$ curves and R_{Hall}–$H_\parallel$ curve, respectively. The dashed blue line is the linear fit of the points.

All experiments were performed at 300 K. The anomalous Hall resistance R_{Hall}, which is proportional to the perpendicular component of the magnetization, was measured with a dc current of 300 μA to obtain the magnetization curves. A tensile stress parallel to the current (x-direction) was applied to the film with a screw-driven tensile machine [Fig. 2(a)]. Both ends of the rectangular sample piece were fixed to the tensile machine by grippers with an initial distance of $d_i \sim 5$ mm. The distance could be controlled by the screw. The increase in distance between the grippers, Δd, was measured with a microscope. A conductive epoxy was used to connect copper wires to electrode pads on the Hall bar device. The strain distribution of the sample with 200-μm-height half-ellipsoid conductive epoxy electrodes was calculated by the finite-element method (FEM). The results are shown in Figs. 2(b) and 2(c). Here, we assumed that the sample consisted of only the PEN substrate and conductive epoxy electrodes because the total thickness of the metallic layers was negligibly small (approximately 1/5000 that of the PEN substrate). A linear-elastic FEM calculation was conducted with a three-dimensional (3D) solid model using Solidworks©. We used Young's modulus and Poisson's ratio of 6.1 GPa and 0.43 for the PEN, and 2.41 GPa and 0.35 for the epoxy, respectively. The FEM calculation revealed that the tensile strain at the center of the Hall bar was 1.08 times larger than the nominal strain because of the existence of the conductive epoxy electrodes. The variation in tensile strain where magnetization information was detected by Hall probes was less than ±0.001%. Therefore, the tensile strain in the present samples, ε_x, was $\varepsilon_x = \Delta d/d_i \times 1.08$. The compressive strain in the orthogonal direction, ε_y, was ~1.10 times larger than that expected in the PEN substrate without the conductive epoxy electrodes. Accordingly, its effective Poisson's ratio became 1.10/1.08 ~ 1.02 times larger under the influence of the electrodes; the observed difference is negligible.

Figure 3(a) shows the magnetization curves of the TFC sample observed at R_{Hall} under the applied strain. Here, a perpendicular magnetic field $H_\perp$ was used to measure the curves. As ε_x increased, the hysteresis of the R_{Hall}–$H_\perp$ curve vanished, i.e., the perpendicular direction became the hard axis. As ε_x decreased, the coercivity H_c and squareness ratio (remanent R_{Hall} divided by the saturated R_{Hall}) recovered to their initial values, as shown in Fig. 3(b). That is, the easy axis switched entirely and reversibly from the perpendicular direction to the in-plane direction with an external stress. Figure 3(c) shows a plot of the uniaxial PMA energy constant K_u with respect to ε_x. K_u ($= 3.4 \times 10^4$ J/m^3) with $\varepsilon_x = 0\%$ was determined from the hard axis magnetization curve reproduced from the R_{Hall}–$H_\parallel$ curve,[20] where $H_\parallel$ is the in-plane magnetic field in the x-direction. The saturation magnetization of the sample (0.47 T) was measured to determine K_u using a superconducting quantum interference magnetometer. When the sample had the in-plane easy axis under a finite ε_x, K_u, as indicated by red points in Fig. 3(c), was determined from the R_{Hall}–$H_\perp$ curve under the assumption that the saturation magnetization was independent of ε_x. From the result, the magnitude of the change in K_u (ΔK_u) of 1.2×10^5 J/m^3 was obtained with $\varepsilon_x = 2\%$.

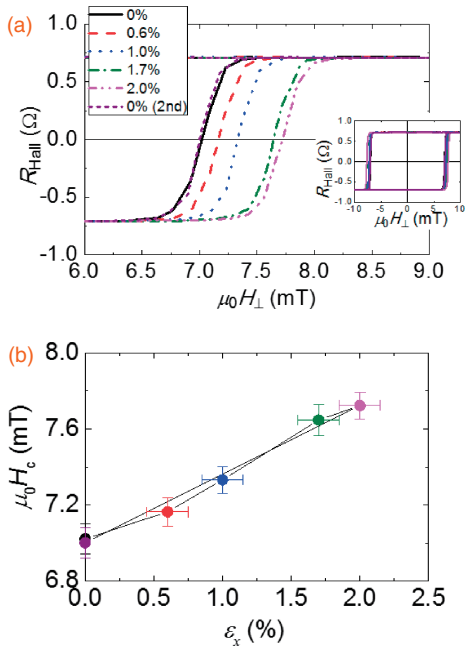

Fig. 4. (a) R_{Hall}–$H_\perp$ curves around H_c of the Pt/Co/Pt ($t_{Co} = 0.8$ nm) sample under various strains. The entire curves are shown in the inset. (b) Dependence of H_c of Pt/Co/Pt ($t_{Co} = 0.8$ nm) sample on ε_x.

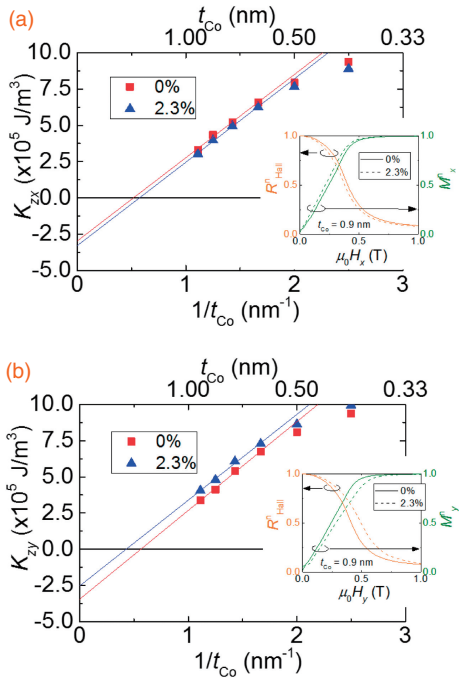

Fig. 5. $1/t_{Co}$ dependences of (a) K_{zx} and (b) K_{zy} in Pt/Co/Pt samples under $\varepsilon_x = 0$ and 2.3%. Normalized Hall resistance R^n_{Hall} and in-plane magnetization $M^n_{x(y)}$ curves under H_x [inset in (a)] and H_y [inset in (b)] with $\varepsilon_x = 0\%$ (solid line) and 2.3% (dashed line) in the sample of $t_{Co} = 0.9$ nm.

Figure 4(a) shows the R_{Hall} of the Pt/Co/Pt sample ($t_{Co} = 0.8$ nm) under various strains. All of the curves show a square hysteresis loop resulting from the PMA. H_c increased with ε_x and recovered to its initial value when the stress was removed [Fig. 4(b)]. In the Pt/Co/Pt samples with various t_{Co} values, the PMA energy constants K_{zx} and K_{zy} were determined by applying an in-plane magnetic field to the x-direction (H_x) and y-direction (H_y), respectively, under $\varepsilon_x = 0$ and 2.3%. The normalized R_{Hall}–$H_{x(y)}$ and hard axis magnetization curves reproduced from them in the sample of $t_{Co} = 0.9$ nm under $\varepsilon_x = 0$ and 2.3% are shown in the insets of Figs. 5(a) and 5(b). The average of the measured saturation magnetizations (1.9 T) of the samples with various t_{Co} values was used to calculate K_{zx} and K_{zy}. Here, we note that the induced moment in the Pt layer by the ferromagnetic proximity effect[21] was neglected to determine the saturation magnetization. K_{zx} and K_{zy} respectively decreased and increased with the application of ε_x at all t_{Co} values [Figs. 5(a) and 5(b)]. Linear fitting in the region $0.6 \le t_{Co} \le 0.9$ nm shown in Figs. 5(a) and 5(b), where the points seemed linear, was performed to distinguish the volume contribution to the PMA energy $K_{zx(zy),v}$ (intercept) and the interface PMA energy $K_{zx(zy),s}$ (slope) according to the equation $K_{zx(zy)} = K_{zx(zy),v} + 2K_{zx(zy),s}/t_{Co}$.[22] The deviation of the points at smaller t_{Co} values may be attributed to a decrease in Curie temperature,[23] an internal strain due to the lattice mismatch,[24] or interfacial mixing.[25] By linear fitting, the MA energy constants were determined to be $K_{zx,v} = -(3.0 \pm 0.4) \times 10^5$ J/m^3, $K_{zy,v} = -(3.4 \pm 0.3) \times 10^5$ J/m^3, $K_{zx,s} = 0.29 \pm 0.01$ mJ/m^2, and $K_{zy,s} = 0.31 \pm 0.01$ mJ/m^2 when $\varepsilon_x = 0$. The changes in $K_{zx,s}$ and $K_{zy,s}$ were smaller than our experimental error $\sim$0.01 mJ/m^2, while those in $K_{zx(zy),v}$ were $\Delta K_{zx,v} \sim -3 \times 10^4$ J/m^3 and $\Delta K_{zy,v} \sim 9 \times 10^4$ J/m^3 with $\varepsilon_x = 2.3\%$.

The observed change in MA energy by strain was expected to be caused by the modulation of the magnetoelastic energy. In the TFC sample case, if the TFC layer is assumed to have an isotropic amorphous structure, the following magnetoelastic energy expression can be used: $E^i_{me} = -3\lambda_s Y \varepsilon_x/2$, where λ_s and Y are respectively the magnetostriction constant and Young's modulus of the magnetic layer. By substituting $Y = 65$ GPa, which is the value for amorphous $TbFe_2$,[26] λ_s can be deduced from ΔK_u ($= 1.2 \times 10^5$ J/m^3 with $\varepsilon_x = 2\%$). The estimated value of λ_s was small (6.1×10^{-5}) compared with the previous result determined by the direct measurement of the magnetostriction constant in a TFC film ($\lambda_s = 3.4 \times 10^{-4}$).[19] This may be attributed to the difference in the substrate or thickness of TFC, i.e., our film was much thinner and K_u was also an order of magnitude smaller than those in previous reports.[19,27] The ΔK_u we obtained in the TFC sample (1.2×10^5 J/m^3) was an order of magnitude larger than the result for the DyFeCo film ($\Delta K_u = 2.0 \times 10^4$ J/m^3)[28] deposited on a glass substrate. This is because of the large applied strain despite the small λ_s.

In the Pt/Co/Pt samples, we determined $K_{zx(zy),s}$ and $K_{zx(zy),v}$ individually. The results clearly indicated that the change in PMA was mainly caused by the modulation of not $K_{zx(zy),s}$ but $K_{zx(zy),v}$. The magnetoelastic energy in a cubic structure is generally expressed as

$$E^c_{me} = B_1\left[\varepsilon_{11}\left(\alpha_1^2 - \frac{1}{3}\right) + \varepsilon_{22}\left(\alpha_2^2 - \frac{1}{3}\right) + \varepsilon_{33}\left(\alpha_3^2 - \frac{1}{3}\right)\right] + 2B_2(\varepsilon_{12}\alpha_1\alpha_2 + \varepsilon_{23}\alpha_2\alpha_3 + \varepsilon_{31}\alpha_3\alpha_1), \quad (1)$$

where B_1 and B_2 are the magnetoelastic coupling constants, and α_i and ε_{ij} (i, $j = 1$, 2, and 3) are respectively the direction cosine of the magnetization direction and the strain tensor with respect to the crystal axis. From this equation, the magnetoelastic energy expression in a (111)-oriented polycrystal was derived on the basis of a previous discussion[29] as

follows. When a very thin magnetic film sticks to a substrate, the expansion in the x-direction, ε_x, and the contraction in the y-direction, ε_y, of the magnetic layer correspond to those of the substrate ($\varepsilon_y = -\nu_{\mathrm{sub}}\varepsilon_x$, where $\nu_{\mathrm{sub}} = 0.43$ is the Poisson's ratio of the PEN substrate in the present case). ε_x and ε_y can be used to determine the strain of the magnetic layer for the z-direction (ε_z), which also depends on its own Poisson's ratio ν_{mag}:[30)]

$$\varepsilon_z = -\frac{\nu_{\mathrm{mag}}}{1-\nu_{\mathrm{mag}}}(\varepsilon_x + \varepsilon_y) = -\frac{\nu_{\mathrm{mag}}(1-\nu_{\mathrm{sub}})}{1-\nu_{\mathrm{mag}}}\varepsilon_x.$$

As a result, the MA changes can be derived as

$$\Delta K_{zx,\mathrm{v}} - \Delta K_{zy,\mathrm{v}} = \frac{B_1 + 2B_2}{3}(1+\nu_{\mathrm{sub}})\varepsilon_x, \quad (2)$$

$$\Delta K_{zx,\mathrm{v}} = \left\{ \frac{B_1}{6}(1+\nu_{\mathrm{sub}}) + \frac{B_2}{6}\left[5 - \nu_{\mathrm{sub}} + \frac{6\nu_{\mathrm{mag}}(1-\nu_{\mathrm{sub}})}{1-\nu_{\mathrm{mag}}}\right]\right\}\varepsilon_x. \quad (3)$$

Magnetoelastic coupling constants can be expressed using the magnetostriction constants λ_{100} and λ_{111} and the elastic constant c_{ij} as $B_1 = -3\lambda_{100}(c_{11} - c_{12})/2$ and $B_2 = -3\lambda_{111}c_{44}$. By substituting $\nu_{\mathrm{mag}} = 0.3$ (the value in ordinary metals) and c_{ij} of an fcc Co ($c_{11} = 304$ GPa, $c_{12} = 154$ GPa, and $c_{44} = 75$ GPa[31)]), the magnetostriction constants were estimated to be $\lambda_{100} = 7 \times 10^{-5}$ and $\lambda_{111} = -1 \times 10^{-5}$. These values are roughly the same as those observed on a glass substrate in Pt/Co multilayers.[32)]

As mentioned above, when a Pt/Co/Pt sample is stretched, there should be a compressive strain along the z-direction in the layers, which reduces the distance between the Pt and Co layers. This is expected to cause the change in $K_{zx(zy),\mathrm{s}}$ because an orbital hybridization at the Pt/Co interface is known to be important for interfacial PMA.[33)] The interesting point, however, was that $K_{zx(zy),\mathrm{s}}$ was almost independent of the strain application in the present case within the experimental error ($\sim$0.01 mJ/m^2). By considering this error, the change in $K_{zx(zy),\mathrm{s}}$ was $\sim$3% at most, whereas that in $K_{zx(zy),\mathrm{v}}$ was $\sim$10–30%. To understand the strain effect on $K_{zx(zy),\mathrm{s}}$, further theoretical study is needed.

In conclusion, we prepared TFC and Pt/Co/Pt samples on flexible PEN substrates, and both showed PMA. When a huge (2%) in-plane uniaxial tensile stress was applied, reversible changes in MA were observed. The TFC sample demonstrated a marked switching of the magnetic easy axis owing to the large strain enabled by the high resilience of the flexible substrate/thin metal layers. PMA in Pt/Co/Pt was divided into volume and interfacial contributions using samples with various Co thicknesses. The change in volume contribution to PMA was in accordance with the conventional magnetoelastic energy modulation, while the interface MA remained almost constant.

Acknowledgments The authors thank S. Ono, A. Tsukazaki, and K. Nakamura for technical help and useful discussion. This work was partially supported by Grants-in-Aid for Scientific Research (S) (25220604), Specially Promoted Research (15H05702) from JSPS, the Murata Science Foundation, and the Toyota Technological Institute Nano Technology Hub in "Nanotechnology Platform Project" sponsored by MEXT. T.T. was partially supported by Grants-in-Aid for Scientific Research on Priority Areas (26107533 and 26102012) and Specially Promoted Research (25000003) from JSPS.

1) A. Itoh, H. Uekusa, Y. Tarusawa, F. Inoue, and K. Kawanishi, J. Magn. Magn. Mater. **35**, 241 (1983).
2) C. Chappert and P. Bruno, J. Appl. Phys. **64**, 5736 (1988).
3) M. Overby, A. Chernyshov, L. P. Rokhinson, X. Liu, and J. K. Furdyna, Appl. Phys. Lett. **92**, 192501 (2008).
4) A. Brandlmaier, S. Geprägs, M. Weiler, A. Boger, M. Opel, H. Huebl, C. Bihler, M. S. Brandt, B. Botters, D. Grundler, R. Gross, and S. T. B. Goennenwein, Phys. Rev. B **77**, 104445 (2008).
5) A. W. Rushforth, E. De Ranieri, J. Zemen, J. Wunderlich, K. W. Edmonds, C. S. King, E. Ahmad, R. P. Campion, C. T. Foxon, B. L. Gallagher, K. Výborný, J. Kučera, and T. Jungwirth, Phys. Rev. B **78**, 085314 (2008).
6) M. Weiler, A. Brandlmaier, S. Geprägs, M. Althammer, M. Opel, C. Bihler, H. Huebl, M. S. Brandt, R. Gross, and S. T. B. Goennenwein, New J. Phys. **11**, 013021 (2009).
7) P. M. Shepley, A. W. Rushforth, M. Wang, G. Burnell, and T. A. Moore, Sci. Rep. **5**, 7921 (2015).
8) F. Zighem, D. Faurie, S. Mercone, M. Belmeguenai, and H. Haddadi, J. Appl. Phys. **114**, 073902 (2013).
9) M. Gueye, B. M. Wague, F. Zighem, M. Belmeguenai, M. S. Gabor, T. Petrisor, C. Tiusan, S. Mercone, and D. Faurie, Appl. Phys. Lett. **105**, 062409 (2014).
10) S. S. P. Parkin, Appl. Phys. Lett. **69**, 3092 (1996).
11) T. Uhrmann, L. Bär, T. Dimopoulos, N. Wiese, M. Rührig, and A. Lechner, J. Magn. Magn. Mater. **307**, 209 (2006).
12) Y. F. Chen, Y. Mei, R. Kaltofen, J. I. Mönch, J. Schumann, J. Freudenberger, H. J. Klauß, and O. G. Schmidt, Adv. Mater. **20**, 3224 (2008).
13) C. Barraud, C. Deranlot, P. Seneor, R. Mattana, B. Dlubak, S. Fusil, K. Bouzehouane, D. Deneuve, F. Petroff, and A. Fert, Appl. Phys. Lett. **96**, 072502 (2010).
14) A. Bedoya-Pinto, M. Donolato, M. Gobbi, L. E. Hueso, and P. Vavassori, Appl. Phys. Lett. **104**, 062412 (2014).
15) A. Kirihara, Y. Nakamura, S. Yorozu, K. Uchida, and E. Saitoh, U.S. Patent 0312802 (2013).
16) W. D. Nix, Metall. Trans. A **20**, 2217 (1989).
17) P. Fredriksson and P. Gudmundson, Int. J. Plast. **21**, 1834 (2005).
18) D. Y. W. Yu and F. Spaepen, J. Appl. Phys. **95**, 2991 (2004).
19) T. M. Danh, N. H. Duc, H. N. Thanh, and J. Teillet, J. Appl. Phys. **87**, 7208 (2000).
20) K. Yamada, H. Kakizakai, K. Shimamura, M. Kawaguchi, S. Fukami, N. Ishiwata, D. Chiba, and T. Ono, Appl. Phys. Express **6**, 073004 (2013).
21) M. Suzuki, H. Muraoka, Y. Inaba, H. Miyagawa, N. Kawamura, T. Shimatsu, H. Maruyama, N. Ishimatsu, Y. Isohama, and Y. Sonobe, Phys. Rev. B **72**, 054430 (2005).
22) P. F. Carcia, J. Appl. Phys. **63**, 5066 (1988).
23) C.-J. Lin, G. L. Gorman, C. H. Lee, R. F. C. Farrow, E. E. Marinero, H. V. Do, H. Notarys, and C. J. Chien, J. Magn. Magn. Mater. **93**, 194 (1991).
24) C. Canedy, X. Li, and G. Xiao, Phys. Rev. B **62**, 508 (2000).
25) S. Hashimoto, Y. Ochiai, and K. Aso, J. Appl. Phys. **66**, 4909 (1989).
26) D. W. Forester, C. Vittoria, J. Schelleng, and P. Lubitz, J. Appl. Phys. **49**, 1966 (1978).
27) H. Awano, K. Ogata, H. Ohlsen, and M. Ojima, J. Magn. Soc. Jpn. **19**, 221 (1995).
28) S. Nakagawa, M. Yamada, and N. Tokuriki, IEEE Trans. Magn. **42**, 3773 (2006).
29) H. Takahashi, S. Tsunashima, S. Iwata, and S. Uchiyama, Jpn. J. Appl. Phys. **32**, L1328 (1993).
30) P. Manchanda, U. Singh, S. Adenwalla, A. Kashyap, and R. Skomski, IEEE Trans. Magn. **50**, 2504804 (2014).
31) *Kinzoku Data Book*, ed. Japan Institute of Metals (Maruzen, Tokyo, 1974) p. 35 [in Japanese].
32) H. Takahashi, S. Tsunashima, S. Iwata, and S. Uchiyama, J. Magn. Magn. Mater. **126**, 282 (1993).
33) N. Nakajima, T. Koide, T. Shidara, H. Miyauchi, H. Fukutani, A. Fujimori, K. Iio, T. Katayama, M. Nývlt, and Y. Suzuki, Phys. Rev. Lett. **81**, 5229 (1998).